Relationship between Q-factor and sample damping for contact resonance atomic force microscope measurement of viscoelastic properties

P. A. Yuya,[1] D. C. Hurley,[2] and J. A. Turner[1,a)]
[1]*Department of Engineering Mechanics, University of Nebraska-Lincoln W317.4 Nebraska Hall, Lincoln, Nebraska 68588-0526, USA*
[2]*Materials Reliability Division, National Institute of Standards and Technology, Boulder, Colorado 80305, USA*

(Received 15 February 2011; accepted 18 April 2011; published online 8 June 2011)

Contact resonance AFM characterization techniques rely on the dynamics of the cantilever as it vibrates while in contact with the sample. In this article, the dependence of the quality factor of the vibration modes on the sample properties is shown to be a complex combination of beam and sample properties as well as the applied static tip force. Here the tip-sample interaction is represented as a linear spring and viscous dashpot as a model for sample (or contact) stiffness and damping. It is shown that the quality factor alone cannot be used to infer the damping directly. Experimental results for polystyrene and polypropylene are found to be in good agreement with predictions from the model developed. These results form the basis for mapping viscoelastic properties with nanoscale resolution. © *2011 American Institute of Physics*. [doi:10.1063/1.3592966]

I. INTRODUCTION

Although the atomic force microscope (AFM)[1] was originally developed for topography imaging, it has more recently been exploited for characterization of mechanical properties. Impressive quantitative and numerous qualitative results have been reported with various modifications of the basic AFM system.[2–9] One such modification, contact resonance force microscopy (CR-FM)[10–12] has become an increasingly important technique for characterizing mechanical properties of materials at submicrometer scales. CR-FM methods use the resonant modes of the AFM cantilever in order to evaluate near-surface mechanical properties.[2,3,5] The initial CR-FM work used the resonant frequencies alone, without consideration of the complete spectral response (i.e., peak width), in order to quantify local elastic properties. Recently,[13] the complete resonance was fit in order to quantify the viscoelastic response of the material. That work introduced the possibility of quantitative mapping of storage and loss moduli with AFM spatial resolution. The connection between the material storage and loss moduli and the resonant frequency and the peak width is often used in dynamic nanoindentation work to quantify viscoelastic properties.[14,15] However, the dynamical system of the instrument is much simpler for nanoindentation because it is often designed to possess only one degree of freedom. Quantitative mapping of viscoelastic properties by AFM is still a challenge because the properties of the sample are convolved with the dynamics of the AFM cantilever beam.[3,13,16,17] Therefore quantitative mapping of the viscoelastic properties of the sample is only possible if the vibrational dynamics of the cantilever-tip-sample combination are well understood.

In this article, we highlight the importance of the cantilever beam dynamics with respect to extraction of the viscoelastic properties of a sample. The quality factor Q for the contact modes of the beam is not proportional to the sample damping and must be determined with respect to its relation with the complex wave numbers of the cantilever. This theoretical approach leads to a method for mapping simultaneously the storage and loss moduli of a sample with CR-FM if the contact resonance and Q values can be simultaneously measured as the tip scans across the sample surface. Such measurements are now possible with a variety of methods[16,18,19] similar to those for imaging elastic properties alone.[20]

II. THEORY

An AFM cantilever beam (with modulus E, density ρ cross-sectional area A, bending moment of inertia I, length L) in contact with a viscoelastic surface is modeled as shown in Fig. 1 where $q(x, t)$ is the displacement of the point x at time t. For simplicity, the tip-sample interaction is modeled as a Kelvin–Voigt element, which is assumed to represent the response of the material alone (rather than the contact). More complex tip-sample interaction models may be needed for specific applications, but this simplified case allows our main points to be clearly made with respect to a large class of materials. In the case of a harmonic displacement, the complex force at the position of the tip is given by $P_{complex} = (k + i\omega c)q(L_1, t)$, where L_1 is the position of the tip from the clamped end, k is the real part and ωc is the imaginary part of the contact stiffness. The flexural motion of the cantilever is often modeled with the Euler–Bernoulli beam equation for which the solution in relation to specific CR-FM applications can be found elsewhere.[3,13,17] Here we focus on the response of the beam to a harmonic force excitation (magnitude F_D; frequency ω) applied at the tip. The displacement of the beam can be expressed as a modal expansion of the form

a)Author to whom correspondence should be addressed. Electronic mail: jaturner@unl.edu.

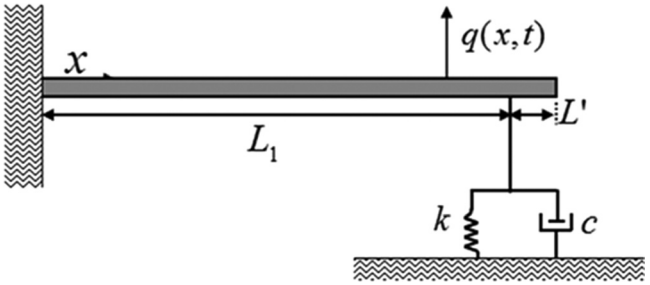

FIG. 1. Mechanical model of an AFM cantilever tip in contact with a viscoelastic surface. The interaction at the AFM tip is approximated by a linear spring-dashpot system that represents the viscoelastic response of the sample.

$$q(x,t) = \frac{F_D e^{i\omega t}}{m_b} \sum_{n=1}^{\infty} \frac{Y_n(L_1)Y_n(x)}{\left[N\gamma_n^4 - \omega^2 + i\omega\overline{\chi}\right]} \quad (\mathrm{n} = 1,2,3\ldots\infty). \quad (1)$$

Here, n are the mode numbers, $m_b = \rho AL$ is mass of the beam, $N = EI/m_b L^3$ and $\overline{\chi} = \chi/\rho \mathrm{A}$ are dimensionless beam constants (where χ represents the assumed viscous damping in the beam), and $\gamma_n = \lambda_n L$ are the normalized wavenumbers. The mode shapes (spatial eigenfunctions) are defined in general form as. $Y_n(x) = \{[\sin(\lambda_n \mathrm{L}) - \sinh(\lambda_n L)]/[\cos(\lambda_n L) + \cosh(\lambda_n L)]\}[\sin(\lambda_n x) - \sinh(\lambda_n x)] + [\cos(\lambda_n x) - \cosh(\lambda_n x)]$ with the shape determined by the wavenumber λ_n. The final aspect of the beam model arises when the boundary conditions (at $x = 0$, L) and continuity conditions (at $x = L_1$) are enforced. These operations result in the characteristic equation that governs the wavenumbers. For the system shown in Fig. 1, this equation reduces to

$$\begin{aligned} &\frac{2}{3}(\lambda_n L_1)^3[1 + \cos\lambda_n L \cosh\lambda_n L] \\ &= \left(\alpha + i\beta(\lambda_n L_1)^2\right)\Big[\left(1 + \cos\lambda_n L' \cosh\lambda_n L'\right) \\ &\quad \times (\sinh\lambda_n L_1 \cos\lambda_n L_1 - \sin\lambda_n L_1 \cosh\lambda_n L_1) \\ &\quad + (1 - \cos\lambda_n L_1 \cosh\lambda_n L_1)\left(\sin\lambda_n L' \cosh\lambda_n L' \right. \\ &\quad \left. - \cos\lambda_n L' \sinh\lambda_n L'\right)\Big], \end{aligned} \quad (2)$$

where $\alpha = k/k_c$ is the dimensionless stiffness and $\beta = c\sqrt{L_1^2/(9EI\rho A)}$ is the dimensionless damping, both of which are attributed here to the sample (although it is recognized that stiffness and damping may arise in the contact itself due to effects such as adhesion).[21,22] Equations (1) and (2) form the basis for the discussion that follows. In particular, it should be noted that the sample damping β does not appear directly in the beam response, Eq. (1).

To understand the relation between sample damping and the value of Q for a given mode, we first assume that the response of the cantilever is near one of the resonances, $\omega \approx \omega_n$, such that the nth-mode behavior dominates. The other modes of the cantilever that are off resonance will not be significantly excited and thus can be neglected. The response at the position of the laser ($x = x_0$) is then

$$q(x_0,t) = A_n e^{i\omega t}\left(\frac{1}{N\gamma_n^4 - \omega^2 + i\omega\overline{\chi}}\right), \quad (3)$$

where the modal amplitude $A_n = F_D Y_n(L_1)Y_n(x_0)/m_b$ depends on the mode shape at the positions of the tip and laser. Equation (3) clearly has the typical damped Lorentzian form as expected. Next, the relation between the modal frequency and damping is found through the wavenumber. The dimensionless complex wavenumbers are defined such that $\gamma_n = a_n + ib_n$, where a_n and b_n are real constants. This form is substituted into Eq. (3) and rearranged, taking in consideration that $b_n \ll a_n$, for the case of small damping. Equation (3) then becomes

$$q(x_0,t) \approx \frac{A_n e^{i\omega t}}{\left(Na_n^4 - \omega^2\right) + i\left(\omega\overline{\chi} + 4Na_n^3 b_n\right)}. \quad (4)$$

The resonant frequency of the nth mode is determined from the real part of the complex wavenumber a_n of that particular mode and the beam damping is increased from $\overline{\chi}$ (for the free beam) by an amount $4Na_n^3 b_n/\omega_n$ (note the dependence on a_n). At this stage, it is convenient to define the dimensionless frequency response function, $G(i\omega)$ as

$$G(i\omega) = \frac{1}{\left(1 - \omega^2/\omega_n^2\right) + i\left(\omega\overline{\chi} + 4\omega_n^2 b_n/a_n\right)/\omega_n^2}, \quad (5)$$

where $\omega_n^2 = Na_n^4$ is the natural frequency. The quality factor Q is defined as the maximum of the magnitude of Eq. (5), $|G(i\omega)|_{\max}$. For small damping, this peak occurs when $\omega \approx \omega_n$ such that Q for the nth mode is written as

$$Q_n = |G(i\omega)|_{\max} = |G(i\omega)|_{\omega=\omega_n} = \frac{\omega_n a_n}{(a_n\overline{\chi} + 4\omega_n b_n)}. \quad (6)$$

Thus we see that for a given mode, Q^{-1} can be decomposed into two parts:

$$(Q_n)^{-1} = \left(Q_n^{\mathrm{free}}\right)^{-1} + \left(Q_n^{\mathrm{sample}}\right)^{-1},$$

where $\left(Q_n^{\mathrm{free}}\right)^{-1} = \overline{\chi}/\omega_n$ is associated with the damping of the cantilever alone and $\left(Q_n^{\mathrm{sample}}\right)^{-1} = 4\ b_n/a_n$ quantifies the damping from the sample. Although such a decomposition may be expected, the form for $\left(Q_n^{\mathrm{sample}}\right)^{-1}$ is not intuitive because it is related directly to the wavenumber rather than directly to the sample damping. This result is a consequence of the boundary value problem solved—the damping of a specific mode arises from a local interaction that depends on the amplitude of the eigenfunction (mode shape) at the tip position. Thus, the modal damping is a complex convolution between the beam response and the damping at the tip. Most importantly, it should be emphasized that for a given mode, the *quality factor Q alone cannot be used to infer the sample damping directly*. Thus the sample damping β must be found by means of a two-step process. First, the measured values of ω_n and Q_n for a given mode are used to determine the components of the complex wave number a_n and b_n. Then the characteristic equation, Eq. (2), is used to determine the stiffness α and damping β. Results are now presented to highlight trends in quality factor as a function of sample properties. Although both ω_n and Q_n are functions of both α and β (3D surfaces), the results shown here are restricted to 2D parametric results for Q_n^{sample} only.

The curves shown in Fig. 2 reveal the dependence of Q_n^{sample} on dimensionless stiffness α as predicted by our model for several values of dimensionless damping β for the first, second, and third modes (note the log-log scale). Several trends in the theoretical curves should be noted. First, it is clear that the relationship between modal Q_n^{sample} and sample damping β is complicated by a dependence on the applied load. Although low values of α (i.e., small load relative to sample stiffness) give a region in which the value of Q_n^{sample} is nearly constant, Q_n^{sample} is, in general, not proportional to β. In fact, most experiments are operated in the region for which these curves are not horizontal (with α in the range of 50-100). Close examination of results for small α (e.g., mode 3) reveals that the quality factor decreases slightly as α increases, a result that is counterintuitive. Also the modal Q_n^{sample} for all values of β converge for large α (large load relative to sample stiffness). Such a trend agrees with experimental observations[3] in which resonances narrow with increasing load on a given sample. These results are shown in a slightly different format in Fig. 3, in which Q_n^{sample} is plotted versus β for constant values of α (note the log-log scale). In this case, it is very apparent that Q_n^{sample} is not proportional to β for any region of constant α. Figures 2 and 3 also highlight the dependence of the results on mode number. Such dependence is important in order to optimize measurements. Choosing an appropriate mode can greatly enhance image contrast and measurement sensitivity.[3,23]

III. EXPERIMENTS

Experimental results are now presented to confirm the validity of the model. CR-FM measurement methods have been described in detail elsewhere.[12] Spectra (cantilever amplitude versus frequency) are acquired for the cantilever in free space and with the tip in stationary contact with two polymers: polystyrene (PS) and polypropylene (PP). Rectangular, single-crystal silicon cantilevers are used with nominal length $L = 225$ μm, mean width $w = 30$ μm, thickness $b = 3$ μm, and spring constant $k_c = 2.8$ N/m. The frequency of the first flexural mode in free space is approximately 66 kHz for the cantilevers used (experimental data for the free resonances are shown in Table I). Contact-resonance spectra are obtained for both samples at several different values of applied load between approximately 100 nN and 1 μN. Measurements are made with the second and third flexural eigenmodes of the cantilever. Contact resonance spectra are acquired by first bringing the cantilever tip into contact with the sample at the specified deflection, then performing the frequency sweep and recording the photodiode voltage, and finally retracting the tip. Acquisition of each spectrum is performed in less than 2 s. In this way, the effect of creep is minimized. Example spectra for mode 2 on PS are shown in Fig. 4 for four different load levels (approximately, 140−224 nN). These results show that Q_n^{sample} changes for

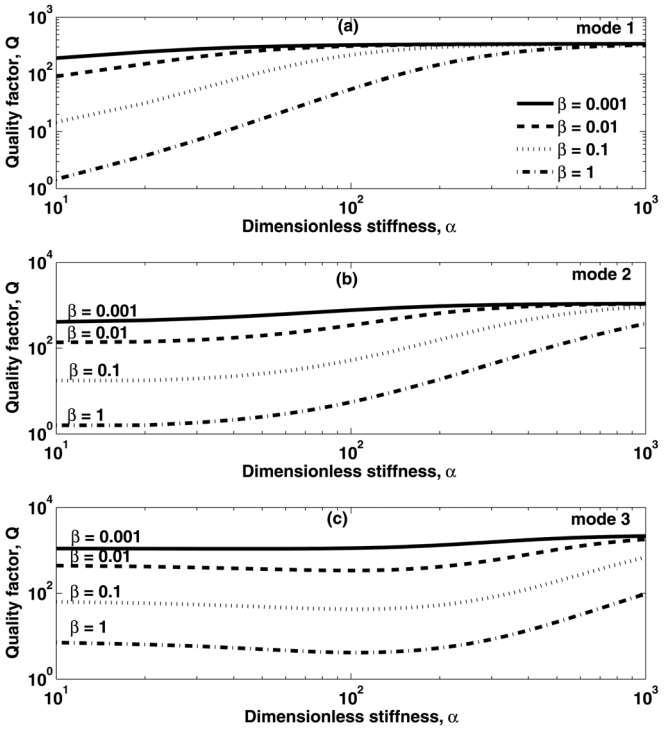

FIG. 2. Dependence of sample quality factor as a function of dimensionless sample stiffness α for various values of dimensionless sample damping β. Results are shown for the first three modes.

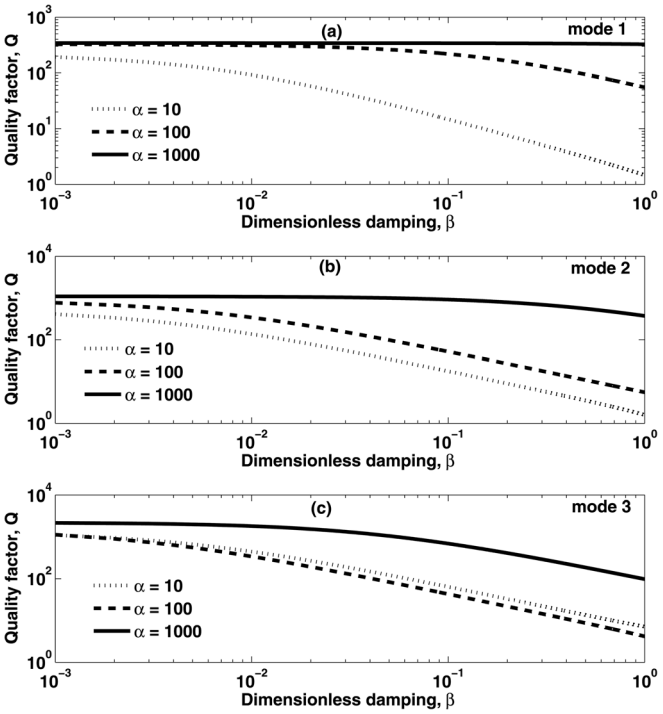

FIG. 3. Dependence of sample quality factor as a function of dimensionless contact damping β for various values of dimensionless sample stiffness α. Results are shown for the first three modes.

TABLE I. Example results for free vibrations of the cantilevers used for the experiments.

Sample	mode 2				mode 3			
	f_2^{free} (kHz)	Q_2^{free}	N (s^{-2})	$\overline{\chi}$ (s^{-1})	f_3^{free} (kHz)	Q_3^{free}	N (s^{-2})	$\overline{\chi}$ (s^{-1})
PS	424	470	$14.6(10)^9$	5,680	1,190	700	$14.8(10)^9$	10,700
PP	415	378	$14.0(10)^9$	6,890	1,170	626	$14.1(10)^9$	11,700

different applied loads although the sample damping is not expected to change over such a small range of frequency.

To analyze the resonances measured, the following procedure is followed. First, the beam properties are determined from the free resonances. The magnitude of Eq. (5) is fit for values of ω_n and $\overline{\chi}$ with a nonlinear least-squares approach and the known wavenumbers for free vibrations.[13] Contact resonance amplitudes for mode n and mode $n+1$ are used to determine the tip position.[3] For each mode, the wavenumber values are obtained, and the characteristic equation is solved for a fixed value wavenumber as the tip position is varied. The plot of α as a function of the tip position L_1/L is generated for the two modes and their crossing point is taken as the tip position. Finally, Eq. (5), with known beam properties, is used to fit the contact amplitude spectra to determine the wavenumbers (with real part a and imaginary part b). These values are then used in Eq. (2) to find the values of α and β. Results from samples of polypropylene (PP) and polystyrene (PS) samples are shown in Fig. 5 for the second and third modes (the first mode changes little for the range of α and β for these samples). Example results are also given in Table II for several data points. Although these results show only Q, note that both ω_n and Q_n are used to determine α and β for a given mode. The ability of the model to extract sample damping is clear from Fig. 5. The Q value changes for the different values of α, but all results can be fit with a single value of β. Finally, it can be observed that $\omega_2\beta_2 \sim \omega_3\beta_3$ for both PP and PS, a result that suggests a frequency dependence in the material damping.

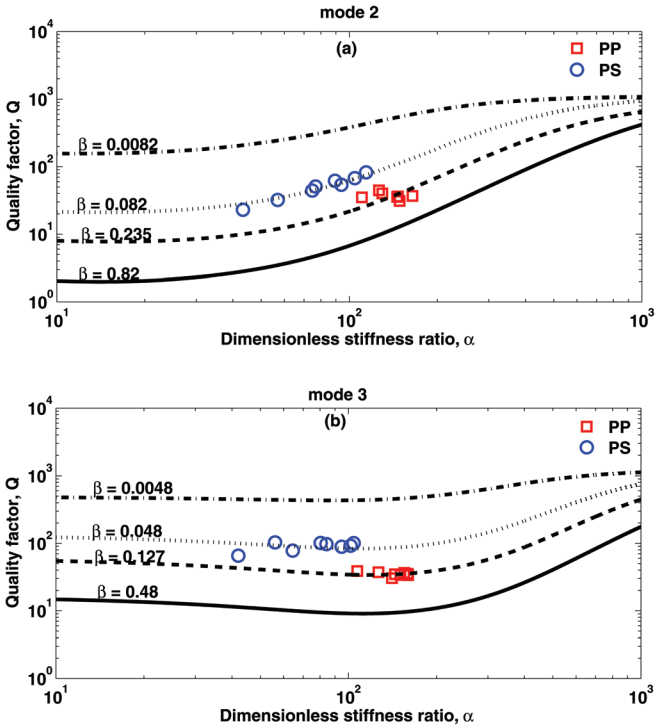

FIG. 5. (Color online) Predicted dependence of quality factor Q for the (a) second and (b) third modes as a function of sample contact stiffness for various values of sample damping β. It is important to note that Q changes with applied load (which changes contact stiffness) even along curves of constant sample damping. The symbols denote experimental results for polypropylene (PP) and polystyrene (PS).

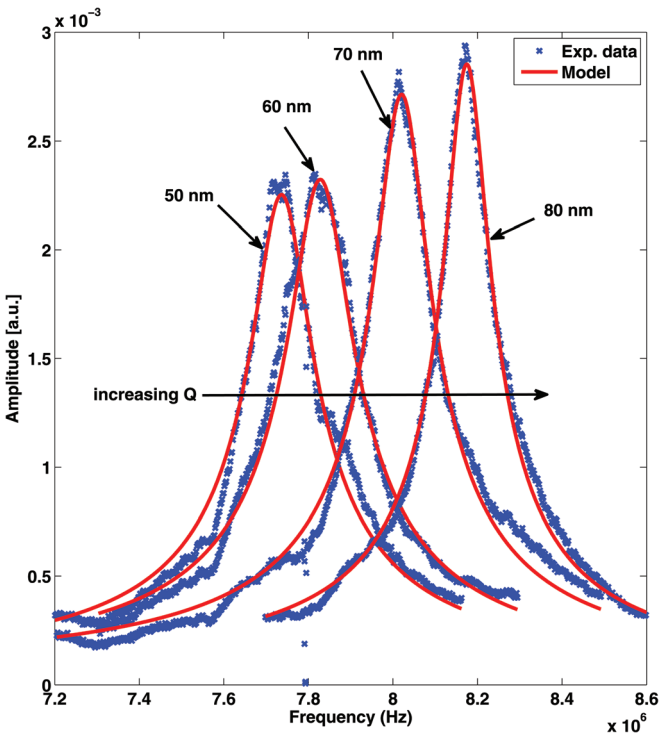

FIG. 4. (Color online) Example contact resonances for mode 2 on a sample of polystyrene. The measurements are made for different values of sample offset which corresponds to a different applied static load (ranging from 140-224 nN). Although sample damping is constant, the Q factor decreases with increasing tip load.

IV. SUMMARY

In this article, the relationship between the Q value and the sample damping has been discussed with respect to contact resonance force microscopy (CR-FM) measurements. It has been shown that Q and damping are related through the dynamics of the AFM beam. The entire beam response must be considered when interpreting resonances obtained from CR-FM. Thus, Q alone cannot be used to deduce sample damping directly. The model presented should prove useful for the development of appropriate tools for quantitative

TABLE II. Example results for some of the data points shown in Figure 5 for polystyrene and polypropylene.

Sample	mode 2				mode 3			
	f_2^{sample} (kHz)	Q_2^{sample}	α	β	f_3^{sample} (kHz)	Q_3^{sample}	α	β
	698	32.1	56.9	0.0875	1290	103	56.1	0.0425
PS	753	50.8	76.7	0.0727	1340	101	80.4	0.0400
	828	82.4	114	0.0740	1390	100	104	0.0390
	808	35.2	110	0.164	1360	38.8	107	0.111
PP	854	35.6	146	0.259	1430	30.4	141	0.145
	857	36.8	164	0.312	1470	33.8	160	0.134

The values of frequency and Q are measured from the experiments; this allows predictions for α and β to be made from the model described (both are dimensionless quantities for stiffness and damping relative to the free response).

mapping of the viscoelastic properties of polymeric and biological samples.

ACKNOWLEDGMENTS

This work was supported in part by the National Science Foundation.

[1]G. Binning, F. Quate, and C. Gerber, Phys. Rev. Lett. **56**, 930 (1986).
[2]K. Yamanaka, A. Noguchi, T. Tsuji, T. Koike, and T. Goto, Surf. Interface Anal. **27**, 600 (1999).
[3]U. Rabe, S. Amelio, E. Kester, V. Scherer, S. Hirsekorn, and W. Arnold, Ultrasonics **38**, 430 (2000).
[4]M. S. Marcus, R. W. Carpick, D. Y. Sasaki, and M. A. Eriksson, Phys. Rev. Lett. **88**, 226103 (2002).
[5]D. C. Hurley, K. Shen, N. M. Jennett, and J. A. Turner, J. Appl. Phys. **94**, 2347 (2003).
[6]R. E. Mahaffy, S. Park, E. Gerde, J. Käs, and C. K. Shih, Biophys. J. **86**, 1777 (2004).
[7]M. Kopycinska-Müller, R. H. Geiss, J. Müller, and D. C. Hurley, Nanotechnology **16**, 703 (2005).
[8]S. Jesse, M. P. Nikiforov, L. T. Germinario and S. V. Kalinin, Appl. Phys. Lett. **93**, 073104 (2008).
[9]A. Caron and W. Arnold, Acta Mater. **57**, 4353 (2009).
[10]U. Rabe and W. Arnold, Appl. Phys. Lett. **64**, 1493 (1994).
[11]U. Rabe "Atomic force acoustic microscopy," In: Applied Scanning Probe Methods, edited by B. Bushan and H. Fuchs (Springer, Berlin, 2006), Vol. II, pp. 37.
[12]D. C. Hurley, "Contact resonance force microscopy techniques for nanomechanical measurements," in: Applied Scanning Probe Methods, edited by B. Bhushan and H. Fuchs (Springer-Verlag, Berlin,: 2009) Vol. XI, pp. 97–138.
[13]P. A. Yuya, D. C. Hurley, and J. A. Turner, J. Appl. Phys. **104**, 074916 (2008).
[14]S. A. Syed Asif, K. J. Wahl, and R. J. Colton, Rev. Sci. Instrum. **70**, 2408 (1999).
[15]G. M. Odegard, T. S. Gates, and H. M. Herring, Exp. Mechan. **45**,130 (2005).
[16]K. Yamanaka, Y. Maruyama, and T. Tsuji, Appl. Phys. Lett. **78**, 1939 (2001).
[17]J. A. Turner, S. Hirsekorn, U. Rabe, and W. Arnold, J. Appl. Phys. **82**, 966 (1997).
[18]S. Jesse, S. V. Kalinin, R. Proksch, A. P. Baddorf, and, B. J. Rodriguez, Nanotechnology **18**, 435503 (2007).
[19]B. J., Rodriguez, C. Callahan, S. V. Kalinin, and R. Proksch, Nanotechnology **18**, 475504 (2007).
[20]A. B. Kos and D. C. Hurley, Measure. Sci. Technol. **19**, 015504 (2008). 1.
[21]D. C. Hurley and J. A. Turner, J. Appl. Phys. **95**, 2403 (2004).
[22]D. C. Hurley, M. Kopycinska-Müller, D. Julthongpiput, and M. J. Fasolka, Appl. Surf. Sci. **253**, 1274 (2006).
[23]J. A. Turner and J. S. Wiehn, Nanotechnology **12**, 322 (2001).